EUROPEAN FUSION DEVELOPMENT AGREEMENT

EFDA–JET–CP(04)02-06

W. Fundamenski, P. Andrew, K. Erents, A. Huber, G. Kirnev, G. Matthews,
R. Pitts, V. Riccardo, S. Sipilä and JET EFDA Contributors

Effect of B×∇B Direction on SOL Energy Transport in JET

Effect of B×∇B Direction on SOL Energy Transport in JET

W. Fundamenski, P. Andrew, K. Erents, A. Huber[1], G. Kirnev[2], G. Matthews, R. Pitts[3], V. Riccardo, S. Sipilä[4] and JET EFDA Contributors*

Euratom/UKAEA Fusion Association, Culham Science Centre, Abingdon, Oxon, UK
[1]FZJ Julich GmbH/Euratom Institut für Plasmaphysik, TEC, Julich D-52425 Germany
[2]Moscow Nuclear Fusion Institute, RRC "Kurchatov Institute", 123182 Moscow, Russia
[3]CRPP-EPFL, Association Euratom-Confédération Suisse, CH-1015 Lausanne, Switzerland
[4]Helsinki U. of Technology, Euratom-Tekes Assoc., POB 2200, FIN-02015 HUT, Finland
** See annex of J. Pamela et al, "Overview of Recent JET Results and Future Perspectives", Fusion Energy 2002 (Proc. 19th IAEAFusion Energy Conference, Lyon (2002).*

Preprint of Paper to be submitted for publication in Proceedings of the
16th PSI Conference,
(Portland, Maine, USA 24-28 May 2004)

ABSTRACT.
The toroidal field and plasma current were reversed in recent JET experiments. Over 100 discharges were obtained, some with good forward field references. Target power deposition was measured using divertor thermocouples. The poloidal power flow in the SOL were found to depend on the B×∇B direction; radiation asymmetries played a minor role in the power balance. The direction, magnitude and scaling of this poloidal power flow can be explained by classical drift-related heat fluxes (E×B and/or B×∇T) whose relative contribution scales $\rho_{\theta s}/\lambda_{T\sigma}$. Radial transport is largely independent of the B×∇B direction, which together with previous experiments rules in favour of classical ion conduction (no B×∇B dependence) as the dominant SOL radial transport mechanism, and against the ion orbit loss process (strong B×∇B dependence). These results were confirmed by detailed EDGE2D and ASCOT simulations of relevant JET plasmas.

1. INTRODUCTION

The exhaust of power from the core plasma via the Scrape-Off Layer (SOL) and the associated energy fluxes on divertor plates and main chamber limiters, are critical issues for ITER. In the standard ITER operational regime, the type-I H-mode, power exhaust may be divided into steady-state (inter-ELM) and transient (ELM) components. Both of these involve SOL energy transport in the parallel (∥), diamagnetic (∧) and perpendicular/radial (⊥) directions. The first two lie on the flux surface and, provided the system is axis-symmetric ($\partial/\partial\phi \sim 0$), may be combined into a single, poloidal direction, θ. This simplification does not change the fact that edge (both pedestal and SOL) plasma transport with respect to the B-field, occurs in three (∥, ∧, ⊥), rather than two (θ, ⊥), dimensions. The diamagnetic (∧) transport is largely due to classical drifts, which for ITER relevant, low collisionality ($\nu^*_{i,sep} < 5$) plasmas, lie mainly on the flux surfaces [1], and whose sign is determined by the **B**×∇**B** direction; in contrast, ∥ transport is largely independent of **B**×∇**B** direction. Here we define **B**×∇**B**↑(↓) as pointing towards (away from) the X-point, which is otherwise known as the forward (reverse) field direction, fwd-B (rev-B) for short. As a direct consequence, SOL flows (both main species and impurity) and divertor asymmetries (density, temperature, pressure, power and radiation) are dependent on the **B**×∇**B** direction.

Over the past years, a series of dedicated experiments were performed on JET and analysed/modelled [7-11] with the aim of deciphering the underlying SOL energy transport mechanism in fwd-B plasmas, the reference field direction of ITER. Narrow outer target profiles ($\lambda_q \sim 3\text{-}5\rho_i$) were found in the near-SOL, in high power, low $\nu^*_{i,sep}$ D H-modes [11]. The integral power width was found to scale roughly as

$$\lambda_q^{all} \propto A(Z) B_\phi^{-1} q_{95}^{0.6} P_t^{-0.4} n_{e,u}^{0.25} \quad (1)$$

The near-SOL profiles are strongly correlated with the ion heat flux, such that $q_i/q_e > 1$ for $\nu^*_{i,sep} < 5$ [18]. Radial (⊥) electron energy transport is anomalous ($\lambda_{qe} \sim \lambda_q \sim 60\text{-}200\rho_e$) most likely governed by electrostatic turbulence driven by interchange MHD and Alven drift-wave instabilities [18].

Comparison with published theories of $\perp$ energy transport in the SOL, suggests that $\perp$ ion energy transport is governed by (neo-) classical ion conduction [11]. The contribution of neo-classical Ion Orbit Loss (IOL) remains unclear. Kinetic simulations suggest that the observed profiles can be reconciled with IOL provided rather large values of the radial electric field are assumed in the SOL (E_r^{SOL} ~ 30-50 kV/m). However, the predicted IOL target profile $\lambda_q^{IOL} \sim \rho_{\theta,i}$ is in poor agreement with the observed scalings with A(Z), B_ϕ and q_{95}.

To test the above conclusions, specifically to investigate the role of IOL (highly sensitive on the $\mathbf{B}\times\nabla\mathbf{B}$ direction) [9,10] in power exhaust, dedicated rev-B experiments were recently performed on JET. In this study, we report the results and preliminary analysis of these experiments, leaving detailed modelling to a subsequent paper.

2. EXPERIMENTS

The idea of reversing the magnetic field in a tokamak is not new. Such experiments have been performed in the past on nearly all machines, including JET [3-6]. However, much of the reported work deals either with Ω or L-mode plasmas, with a focus on low power, high density regimes [1,2]. In light of low $\nu^*_{i,sep}$ in ITER and recent improvements in divertor thermography, it was felt that new JET experiments providing closely matched forward-reverse pairs of H-mode discharges were desirable. For this purpose, high clearance magnetic configurations were used (described in detail in [9]), allowing the plasma to be slowly lifted as a rigid-body in order to characterise the deposited power profiles on the inner and outer divertors using Langmuir Probes (LP) and embedded ThermoCouples (TC). Both B_ϕ and I_p were reversed, such that the magnetic helicity remained constant.

Four good discharges were obtained: one L-mode and three H-modes at different values of B_ϕ, I_p and P_{heat}. The resulting forward-reverse matched pairs are summarised in Table 1. With the exception of the 2.5 MA/2.4T H-mode, for which Type-I ELMs could not be obtained due to the higher III-I power threshold with rev-B [15], the discharges are fairly well matched in terms of power entering the SOL, $P_{SOL} = P_{heat} - P_{rad}$ and line average density $\langle n_e \rangle$; the majority (60-90%) of this power crosses the separatrix during the inter-ELM phase. Due to progressive wiring failure, the LP coverage was much poorer at the time of the reversed field experiments, hence the ~ sign denoting errors of order ± 50%. The two point model was used to predict the upstream values of T_e and n_e, based on total (TC) heat fluxes to the outer target.

The total (ELM-averaged) deposited energy distribution on the divertor tiles was measured by TC analysis for the matched pairs of shots. The resulting out-in energy asymmetry is plotted vs. P_{SOL} in Fig.1; it is reduced from ~2.65-2.2 for fwd-B to ~1.7-1.9 for rev-B, with the average value roughly constant at 2.1±0.05. The fractional energy asymmetry $\Delta E/\Sigma E \equiv (E_o-E_i)/(E_o+E_i)$ increases roughly linearly with P_{SOL} for H-mode plasmas, and is much larger for L-mode despite a lower power. This was also observed on a large sample (>100 shots) of unmatched fwd-B and rev-B shots from the same experimental campaign [12]. The difference between L and H asymmetries is greatly reduced if the data is plotted vs. the power above the L-H threshold, i.e. $P_{SOL} - P_{LH}$, Figure 1.

In a recent review, the out-in power asymmetries were ascribed to an asymmetry in divertor radiation [2]. To test this hypothesis, the NBI heating power was increased from 2 to 8MW in two matched fwd-B and rev-B JET L-modes (58850, 59557; 2.0MA, 2.4T). The target power was measured using transient analysis of the TC time traces, while careful radiation accounting was obtained using tomographic reconstructions of bolometric lines of sight. The results [13] show that at higher input powers, divertor radiation is less important, and the target power asymmetries reflect actual changes of power flux into the divertor legs. The change of the $P_{div} = P_{target} + P_{rad}$ asymmetry with $\mathbf{B}\times\nabla\mathbf{B}$ direction ($P_{div,o}/P_{div,i}$ ~2.3 vs. ~1.3) suggests this power flux has a component in the diamagnetic direction associated with classical drifts.

Returning to the swept discharges, the TC measured total (ion + electron) deposited power profiles on the inner and outer targets are shown in Fig.2 for the matched pairs of shots, along with peak values qpeak and integral widths λ_q. The peak values are additionally plotted vs. PSOL in Fig.3, together with LP measurements of peak electron heat flux. The out-in peak heat flux asymmetry (both TC and LP) ranges from 5-7 for $\mathbf{B}\times\nabla\mathbf{B}\downarrow$, and 1.7-3.7 for $\mathbf{B}\times\nabla\mathbf{B}\uparrow$. The excess of ion over electron power for fwd-B H-modes, q_{TC}/q_{LP} ~ 2-5, is less pronounced in rev-B, q_{TC}/q_{LP} ~ 1.2-1.8, although the poorer accuracy in the rev-B LP data should be noted.

In order to assess the effect of field reversal, the above (TC) values were plotted vs. the scaling $q_t \sim P_t/\lambda_q$ with λ_q, given by (1), derived from two dozen outer target fwd-B shots (mostly H-modes), Figure 4. Within the measurement errors, the outer target rev-B H-mode points do not substantially differ from the fwd-B scaling, while the inner and L-modes points are only grossly correlated with the scaling. We conclude that under low collisionality (attached) conditions, the power width λ_q is insensitive to the $\mathbf{B}\times\nabla\mathbf{B}$ direction. Since this quantity is directly related to the radial ($\perp$) heat diffusivity, $\lambda_q \sim (\chi_\perp \tau_\parallel)^{1/2}$, we may infer that radial energy transport in the SOL is largely independent of the B´ÑB direction, hence of classical drift effects – a most notable result!

3. DISCUSSION

We are thus faced with three separate observations: a) the average out-ion power asymmetry of both P_{target} and P_{div} increases roughly linearly with P_{SOL}, b) this asymmetry, for the same value P_{SOL}, is less sensitive to field reversal for the H-modes (ELM-averaged), than for L-modes, c) radial (^) energy transport is largely independent of the $\mathbf{B}\times\nabla\mathbf{B}$ direction. Roughly speaking, we find that the $\mathbf{B}\times\nabla\mathbf{B}$ direction affects the poloidal (θ) but not the radial ($\perp$) energy transport. In this section we examine the implications of these results.

There is an overwhelming body of evidence [1,2] to suggest that the majority of the power enters the SOL on the Low Field Side (LFS), near the outer mid-plane (omp); this is a consequence of: a) geometry (larger outboard area), b) Shafranov shift compressing the flux surfaces on LFS, c) bad curvature and the consequent increase in MHD-turbulence on LFS. These effects are independent of the $\mathbf{B}\times\nabla\mathbf{B}$ direction, and with $R_o/R_i \sim L_{||i}/L_{||o} \sim 2$ predict an average out-in power asymmetry P_o/P_i of ~ 2 (1.7 due to surface area alone) in agreement with Fig.1.

In order to explain the $\mathbf{B}\times\nabla\mathbf{B}$ dependence of P_o/P_i, we must consider the effects of drifts on energy transport in the SOL. Chankin [5] derives expressions for the drift related energy fluxes, which can be written as,

$$\begin{aligned}\mathbf{q}_\sigma &\approx 2.5p_\sigma\mathbf{v}_\sigma + 2.5p_\sigma v_{t\sigma}\rho_\sigma\mathbf{b}\times\nabla T_\sigma/T_\sigma \\ \mathbf{v}_\sigma &= v_{||\sigma}\mathbf{b} + \mathbf{v}^E + \mathbf{b}\times(\nabla p_{\perp\sigma} - \mathbf{R})/m_\sigma n_\sigma\Omega_\sigma + \{(v_{t||\sigma}{}^2 - v_{t\perp\sigma}{}^2 + v_{t||\sigma}{}^2)/\Omega_\sigma\}\mathbf{b}\times\mathbf{b}\cdot\nabla\mathbf{b}\end{aligned} \qquad (2)$$

where $\mathbf{b} = \mathbf{B}/B$ is a unit vector, $\mathbf{v}^E \sim (1+0.25\rho_\sigma{}^2\nabla^2)\mathbf{E}\times\mathbf{b}/B \sim \mathbf{E}\times\mathbf{b}/B$ is the electrostatic drift velocity, $v_{t||\sigma} = (T_{||\sigma}/m_\sigma)^{1/2}$ and $v_{t\perp\sigma} = (T_{\perp\sigma}/ms)^{1/2}$ are thermal velocities, $\Omega_\sigma = e_\sigma B/m_\sigma$ is the gyro-frequency, $\rho_\sigma = v_{t\perp\sigma}/\Omega_\sigma \sim v_{t\sigma}/\Omega_\sigma$ the thermal gyro-radius, $\sigma\in\{i,e\}$ the species index, e_σ is the charge ($-e$ for electrons, $+Ze$ for ions). Dominant contributions to the q (strictly speaking $\wedge$) components of (1) arise due to $\mathbf{E}\times\mathbf{B}$ and diamagnetic drifts. We write these explicitly as,

$$q_{\sigma\wedge}{}^E \sim 2.5p_\sigma E_\perp/B_\phi, \quad q_{\sigma\wedge}{}^{\nabla P} \sim 2.5(T_\sigma/e_\sigma B_\phi)\,\nabla_\perp p_{\perp\sigma}, \quad q_{\sigma\wedge}{}^{\nabla T} \sim 2.5(p_\sigma/e_\sigma B_\phi)\nabla_\perp T_\sigma \qquad (3)$$

Basic vector calculus suffices to show that diamagnetic heat fluxes are very nearly divergence free inside the plasma, $\nabla\cdot\mathbf{q}_\sigma{}^{\nabla p} \sim \nabla\cdot\mathbf{q}_\sigma{}^{\nabla T} \sim 0$. As such, they do not affect the energy dynamics of the plasma, which is determined by terms involving $\nabla\cdot\mathbf{q}_\sigma$, and can be neglected in most numerical simulations. This is not to say that these fluxes are fictitious; nor does it imply that they deposit no energy on the divertor targets. It can be shown that the latter does in fact apply to $\mathbf{q}_\sigma{}^{\nabla p}$, due to the $||$ pressure gradient in the magnetic pre-sheath [1,6]. However, the same argument does not hold for $\mathbf{q}_\sigma{}^{\nabla T}$, especially $\mathbf{q}_i{}^{\nabla T}$, since $\nabla_{||}T_i \sim 0$ at the entrance to the pre-sheath [1]. Since typically $T_i/T_e \sim 2$ in the SOL, this implies a net energy deposition on the outer target with $\mathbf{B}\times\nabla\mathbf{B}\downarrow$ due to both the $\mathbf{E}\times\mathbf{B}$ and diamagnetic (conductive) drifts.

To first order, we can estimate the radial E-field as $E_\perp \sim 3\nabla_\perp T_{e,t}$ evaluated at the outer target. Writing the θ component of the $||$ energy flux as $q_{\theta\sigma} = (B_\theta/B)q_{||\sigma}$ with $q_{||\sigma} \sim p_\sigma L_{||}/\tau_{||\sigma}$ and $\tau_{||i} \sim L_{||}/c_s$, $\tau_{||e} \sim L_{||}{}^2/\chi_{||e}$, we find

$$\begin{aligned} q_{i\theta}{}^E/q_{\theta i} &\sim 3\nabla_\perp T_{e,t}/c_s B_\theta \sim 3\rho_{\theta s}/\lambda_{Te,t}, & q_{e\theta}{}^E/q_{\theta e} &\propto \nu^*{}_e\rho_{\theta s}/\lambda_{Te,t}, \\ q_{i\theta}{}^{\nabla T}/q_{\theta i} &\sim \nabla_\perp T_{\sigma,t}/c_s e_\sigma B_\theta \sim \pm\rho_{\theta s}/\lambda_{Ti}, & q_{e\theta}{}^{\nabla T}/q_{\theta e} &\propto \nu^*{}_e\rho_{\theta s}/\lambda_{Te}, \end{aligned} \qquad (4)$$

where $c_s = \{(ZT_e+T_i)/m_i\}^{1/2}$ is the plasma sound speed. Hence the ratio of the poloidal components of the drift and parallel heat fluxes can be estimated as the gyro-radiusnormalised by the temperature gradient length, $\lambda_{T\sigma} \equiv |\nabla\perp T_\sigma/T_\sigma|^{-1}$. Since $\lambda_q \sim 3\text{-}5\rho_i \sim 0.3\text{-}0.5\rho_{\theta i}$ in high power H-modes on JET, with typical $\lambda_{T\sigma} \sim 2\text{-}3\lambda_q$, we can expect $\rho_{\theta i}/\lambda_{Ti} \sim O(1)$ and thus a significant contribution from drift effects for low $\nu^*{}_i$. Using the experimental λ_q (1) as a rough guide for the $\lambda_{T\sigma}$ scaling, we find that the B-dependence cancels leaving a positive, roughly linear, power scaling,

$$\{q_{\sigma\wedge}{}^{E},\ q_{\sigma\wedge}{}^{\nabla T}\}/q_{\wedge\sigma} \propto T_{\sigma,t}{}^{0.5}\ P_{SOL}{}^{0.5}\ n_{e,\,u}{}^{-0.5} \qquad (5)$$

in agreement with experiment, Fig.1 and [12,14]. This strongly suggests that the out-in divertor energy asymmetries are a direct consequence of classical (**E¥B** and/or **B¥—T**) drift-related heat fluxes in the SOL.

To further quantitatify this conclusion, numerical simulations of matched fwd-B and rev-B discharges were performed using the EDGE2D transport code [16], with two sets of assumptions: a) classical drifts, with the exception of divergence free (diamagnetic) terms; no radial pinch; b) radial velocity (pinch) term with $v_\perp$ = 10m/s, directed towards the LFS for fwd-B and HFS for rev-B [14]. In each case, poloidally varrying radial transport coefficients $\{D_\perp, \chi_\perp\}(q)$ were used, to simulate increased transport on the LFS. Both pure D and D+C simulations were performed for each set of assumptions. The results are plotted vs. $P_{SOL}\mathbf{B}/B$ (negative values correspond to $\mathbf{B}\times\nabla\mathbf{B}\downarrow$) in Fig.5; also shown is the experimental data from Fig.1, with P_{SOL} replaced by $P_{SOL}/3$ for the L-mode points and $(P_{SOL}-P_{LH})/3$ for H-mode points, to compensate for the lower density used in the simulations, $n^{eu\ EDGE2D}/n_{eu}{}^{JET} \sim 1/3$. The increase of P_o/P_i with input power is observed in all simulations, with the exception of the pinch velocity in a pure D plasma. Similar agreement is found with a larger L-mode data set [12,14]. This suggests a complicated coupling between mass and energy transport, inwhich classical drifts play a central role.

The role of ion orbit loss, one of the key motivating issues for these experiments, can now be proparely assessed. This effect has been simulated using the guiding centre Monte-Carlo code ASCOT, in realistic JET magnetic geometry. The pedestal and SOL plasma profiles were taken for the fwd-B shot 50401 (2.5MA/2.4T, 12 MW NBI), which has previously been modelled extensively and has the same field, current as the 50379/59691 pair, and similar heating power [9,10]. Self-consistent simulations were perfomred with a 15mm-omp pedestal width, equivalent to $2.5\rho_{\theta i}$ at the outer mid-plane, with $T_{i,ped} \sim 1.1$keV and $T_{i,sep} \sim 400$eV. Three values of $E_{r,SOL}$ were used: 0, 45 and 75 kV/m; only the largest field value yields ion peak powers > 5MW/m^2 as measured for this shot [9,10]. The results are shown in Fig.6. The effect of field reversal on target power profiles is quite dramatic, with the outer profiles drastically broadened and peak values reduced, in contrast to experiment where little change in λ_q was observed, Fig.4. A series of trace simulations were also performed using ASCOT to test the effects of launch location, anomalous diffusion and toroidal field ripple, Table 2. The trends and absolute values of q_o/q_i differ grossly from experiment. The only exception is a combination of IOL subject to additional $D_\perp \sim 1$m^2/s with large values of $E_\perp{}^{SOL} \sim 50$kV/m (an unlikely physical combination); even in this case, although the power asymmetry is reproduced, the shape of the profiles for rev-B is not. We are thus forced to conclude that orbit loss is *not* directly responsible for the observed target profiles. More likely, IOL carries power down the pedestal gradient and into the SOL, where (neo-)classical conduction processes take over.

CONCLUSIONS

What have we learned from the new JET experiments? First, that field reversal affects the poloidal power flow into the divertor and hence power flow in the SOL; radiation asymmetries play a role only in highly collisional plasmas. Second, that the direction, magnitude and scaling of this poloidal power flow can be explained by classical drift-related heat fluxes (**E**×**B** and/or **B**×∇**T**) whose relative contribution can be estimated as rqs/lTs; this conclusion is further backed up by numerical simulations using the EDGE2D code. Third, that radial transport is largely independent of the **B**×∇**B** direction; this key finding weighs heavily in favour of classical ion conduction (no **B**×∇**B** dependence) as the dominant SOL radial transport mechanism, and against the ion orbit loss process (strong **B**×∇**B** dependence). This is confirmed by detailed ASCOT simulations of IOL under realistic JET conditions. The only outstanding issue related to SOL energy transport are therefore issues related to ELMs, which will be the focus of future work.

REFERENCES

[1]. C.S. Pitcher et al., Plasma Phys. Control. Fusion **39** (1997) 779.
[2]. P.C. Stangeby, The Plasma Boundary of Magnetic Fusion Devices, IoP Publishing (2000).
[3]. A. Chankin et al., Plasma Phys. Control. Fusion **36** (1994) 1853.
[4]. A. Chankin et al., Plasma Phys. Control. Fusion **36** (1996) 563.
[5]. A. Chankin, J. Nucl. Mat., **241-243** (1997), 199.
[6]. A. Chankin, J. Nucl. Mat., **290-293** (2001), 518.
[7]. V.Riccardo et al., Plasma Phys. Contr. Fusion, **43** (2001), 881.
[8]. G.F.Matthews et al., J. Nucl. Mat., **290** (2001), 668.
[9]. W.Fundamenski, Plasma Phys. Contr. Fusion, **44** (2002), 761.
[10]. W.Fundamenski et al., J. Nucl. Mat., **313** (2003) 787.
[11]. W. Fundamenski et al., Nuclear Fusion, **44** (2004) 20.
[12]. R. Pitts, these proceedings.
[13]. A. Huber, these proceedings.
[14]. G. Kirnev, these proceedings.
[15]. Y Andrew et al., Plasma Phys. Control. Fusion **46** (2004) 337-347.
[16]. R. Simonini et al., Cont. Plasma Phys., **34** (1994), 347.
[17]. J.A.Heikkinen, Phys. Plasmas, **8** (2001), 2824.
[18]. W.Fundamenski, 11 th European Fusion Physics Workshop, Heraklion, Crete (Dec. 2003).

Shot	B×∇B	Mode	I_p	B_ϕ	q_{95}	$\langle n_e \rangle$	P_{heat}	P_{SOL}	j_s^{in}	j_s^{out}	T_e^{in}	T_e^{out}	T_e^{SOL}	n_e^{SOL}	f_{ELM}	ΔW_{ELM}	P_{ELM}	W_{ped}	$\Delta W/W_{ped}$
50415	↓	L	2.5	2.4	2.7	3.3	4.4	2.7	~2	3.9	~10	18	63	2.32	-	-	-	1.65	-
59589	↑	L	2.5	2.4	2.7	3.3	5.3	4.0	~4	~5	~25	~25	81	3.5	-	-	-	1.53	-
50397	↓	H-I	2.5	2.4	2.7	6.5	15.6	9.5	~2.5	4.0	~8	25	97	1.78	12	330	4	5.6	0.06
59691	↑	H-III	2.5	2.4	2.7	6.2	14.2	11.0	~6.5	~7	~25	~25	98	4.4	~30	~50	1.5	3.9	0.01
56707	↓	H-I	1.5	1.45	2.7	5.0	10.2	6.7	~1.8	2.2	~8	34	78	1.46	10	200	2	2.2	0.09
59592	↑	H-I	1.5	1.45	2.7	4.0	9.4	6.3	~2.5	~6	~20	~20	84	3.0	~40	~50	2	2.3	0.02
56709	↓	H-I	1.5	2.2	4.2	3.9	9.8	7.2	~1.5	1.8	~10	35	102	0.96	20	100	2	2.6	0.04
59697	↑	H-I	1.5	2.2	4.3	3.9	11.9	8.8	~5	~9	~20	~20	109	3.7	20	100	2	2.1	0.05

Table 1: Summary of matched pair discharges; all plasmas are D^+, NBI heated; units: I_p (MA), B (T), P (MW), n_e (10^{19} m^{-3}), T (eV), j_s (10^5 A/m^2), f_{ELM} (Hz), ΔW_{ELM} (kJ), W_{ped} (MJ); also used $L_{\parallel}[m] \cong 50\times(q_{95}/2.6)$.

i-i	i-n	θ_0	ρ_0	$D_\perp^{an}$	$E_\perp^{SOL}$	Γ_o/Γ_i	q_o/q_i	P_o/P_i
0	0	0-2π	0.95-1	0	0	0.37, 5.62	0.27, 12.71	0.32, 15.32
1	0	0-2π	0.95-1	0	0	0.55, 7.18	0.30, 22.26	0.36, 26.73
1	1	0-2π	0.95-1	0	0	0.65, 6.81	0.34, 15.41	0.41, 18.58
1	1	0-2π	0.95-1	0	10	0.90, 4.21	0.39, 12.49	0.47, 15.02
1	1	0-2π	0.95-1	0	20	1.29, 2.63	0.50, 9.55	0.60, 11.53
1	1	0-2π	0.95-1	0	75	5.17, 0.56	1.09, 5.03	1.31, 6.08
1	1	0	1	0	0	9.06, 1.24	6.73, 1.46	8.15, 1.76
1	1	π	1	0	0	0.10, 20.34	0.12, 22.65	0.15, 27.23
1	1	0	0.95-1	0	0	2.22, 2.93	0.91, 7.47	1.10, 8.99
1	1	0	0.95-1	0	75	4.66, 0.81	0.94, 5.40	1.13, 6.50
1	1	0-2π	0.95-1	1	0	2.11, 1.66	1.55, 1.73	1.88, 2.09
1	1	0-2π	0.95-1	1	75	12.85, 0.26	3.83, 1.19	4.61, 1.42
1	1	0-2π	0.95-1	B_{rip}	0	0.67, 6.43	0.44, 15.72	0.53, 18.90
1	1	0-2π	0.95-1	B_{rip}	75	5.26, 0.57	2.22, 4.66	2.69, 5.63

Table 2: ASCOT trace run results: $n_i^{ped} = n_i^{sep} = 1.5e19\ m^{-3}$; $T_i^{ped} = 1keV$; $T_i^{sep} = 168eV$ (omp); Maxwellian f(E, α) with local (n_i, T_i) For 2D (n_i, T_i)) SOL plasma (JET Pulse No: 50401); $\Delta_{ped} = \{0, 15\}$ mm- omp; E_r^{core} = neo- classical. Results are listed for (fwd-B, rev-B).

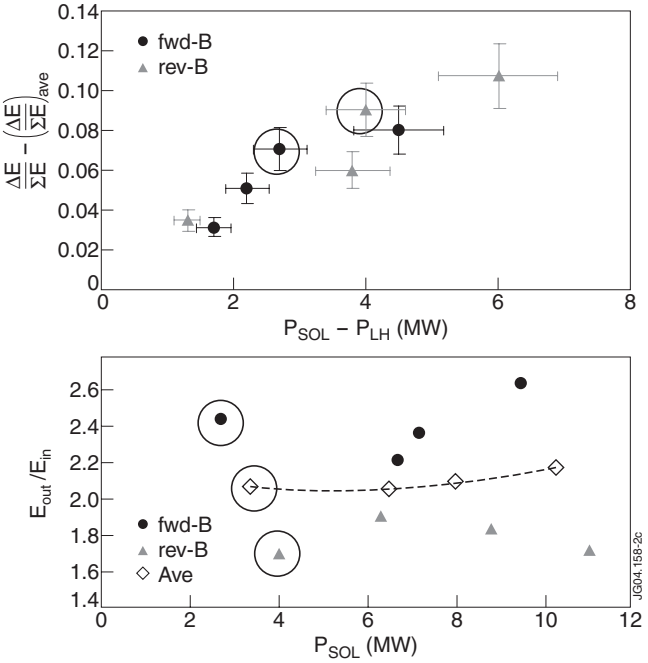

Figure 1: Out-in energy asymmetry vs. power into the SOL, and the $\Delta E/\Sigma E \equiv (E_o-E_i)/(E_o+E_i)$ vs. power above L-H threshold.

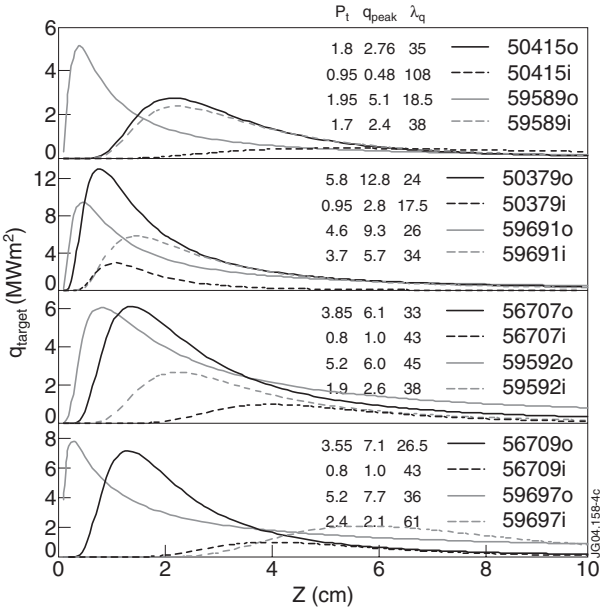

Figure 2: Target power deposition profiles obtained using TC analysis for matched pairs of fwd-B and rev-B shots from Table 1. Plotted vs. vertical distance along the tile.

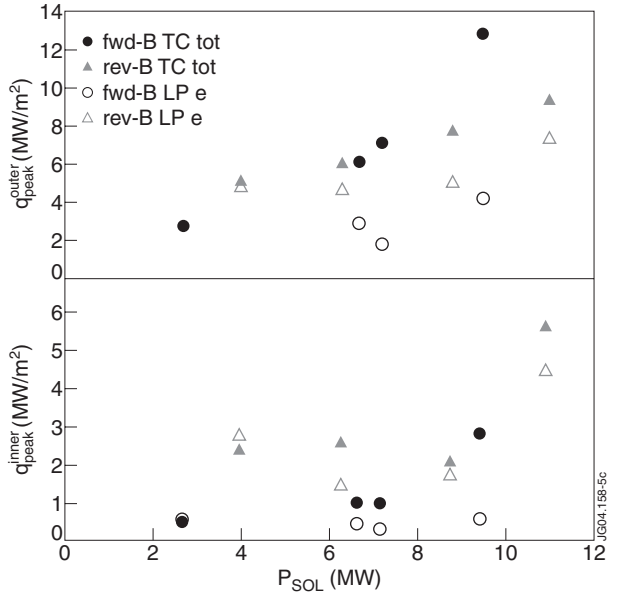

Figure 3. Outer and inner, TC (total) and LP (electron) peak heat load values vs. power into the SOL.

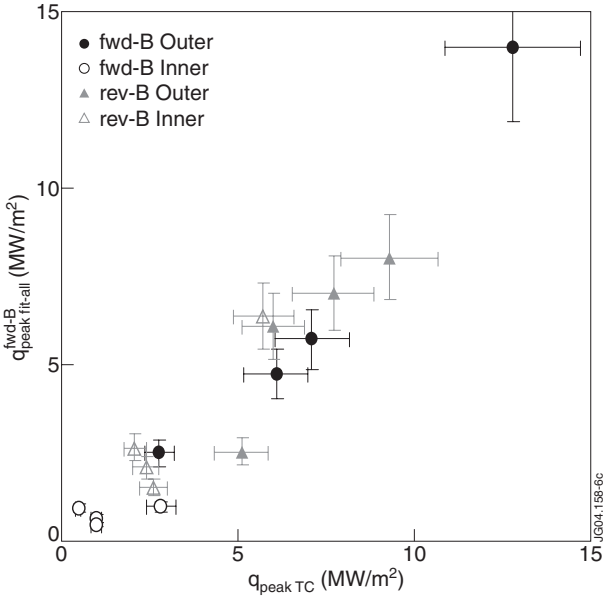

Figure 4. TC measured (total) peak heat loads vs. best fit to all outer, fwd-B, TC data, eq'n (1).

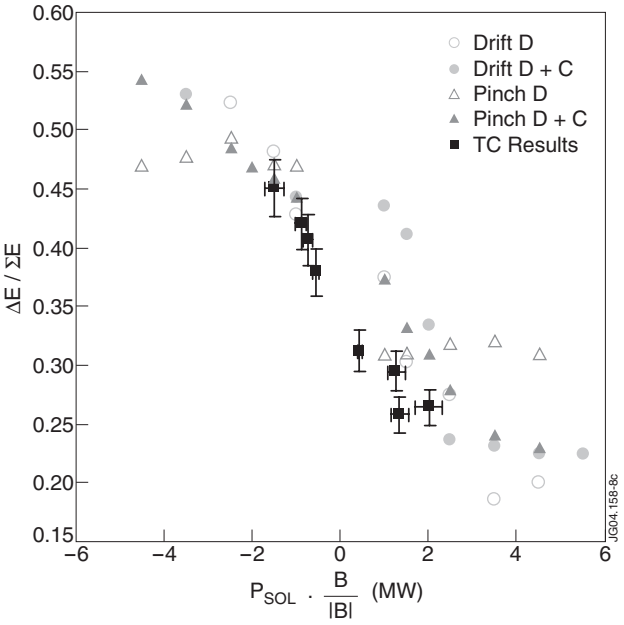

Figure 5: Comparison of EDGE2D modelling to theory with $\Delta E/\Sigma E \equiv (E_o-E_i)/(E_o+E_i)$ vs. power into the SOL.

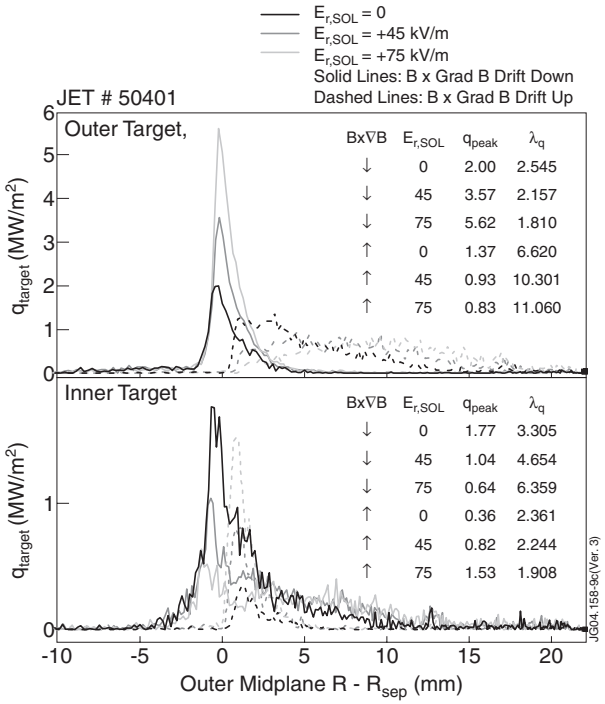

Figure 6: ASCOT modelling of ion orbit loss target heat loads for 2.5MA/2.4T/12MA JET shot (fwd-B vs. rev-B); $E_{r,SOL}$ (kV/m), λ_q(mm-omp)